Hindawi
Geofluids
Volume 2022, Article ID 3292399, 14 pages
https://doi.org/10.1155/2022/3292399

Research Article

Influence of Organic-Inorganic Composition on the Adsorption of Niutitang Formation Shale in Huijunba Syncline

Xiang Xing,[1] **Deliang Fu**,[2] **Zixiang Wang**,[3] **Yang Tian**,[4] **and Lina Sun**[4]

[1]*Hubei Geological Bureau, Hubei Wuhan 430100, China*
[2]*Key Laboratory of Coal Exploration and Comprehensive Utilization, Ministry of Nature and Resources, Shaanxi Coal Geology Group CO., LTD, Shaanxi Xi'an 710021, China*
[3]*Key Laboratory of Exploration Technologies for Oil and Gas Resources (Yangtze University), Ministry of Education, Wuhan 430100, China*
[4]*Hubei Cooperative Innovation Center of Unconventional Oil and Gas, Yangtze University, Hubei Wuhan 430100, China*

Correspondence should be addressed to Deliang Fu; fudl3513@foxmail.com

Received 2 May 2022; Accepted 27 June 2022; Published 16 July 2022

Academic Editor: Wei Sun

To study the influence of different organic-inorganic composition on the adsorption in shale, taking the Niutitang Formation shale in the Huijunba syncline in southern Hanzhong as the research object, based on acid treatment to extract kerogen and wet chemicals. Extracting mineral components by oxidation method, a series of isothermal adsorption experiments were carried out on the original rock, kerogen, and mineral components of the samples. Through the three-dimensional Langmuir model fitting and adsorption thermodynamic calculation method, the adsorption thermodynamic parameters such as the isometric heat of adsorption and the standard adsorption entropy are obtained. The research results show that organic matter is the primary factor affecting the methane adsorption of shale and clay minerals also affect the adsorption to a certain extent. When the burial depth is relatively shallow, diagenesis has a promoting effect on the total amount of adsorption. As the depth increases, the diagenesis will turn into an inhibitory effect on the total amount of adsorption. Through the component weighting method, the lower limit ratio of the adsorbed amount of organic matter to the total amount in the shale is 29.3%~46.7% when the depth reaches to 3000 m, while the upper limit ratio of the adsorption of mineral components is 66.4%~73.6%.

1. Introduction

The adsorption gas content of shale is mainly affected by the total organic matter content (TOC), thermal evolution degree, the type and content of minerals, and other factors. At the same time, the temperature and pressure environment and the moisture of shale are also the main objective factors controlling the adsorption gas amount of shale [1–9]. In fact, the adsorption of natural gas belongs to physical adsorption, which is the retention of methane and other gases on the surface of adsorbent in the adsorption state, and the nanopores of shale are the important physical basis for the methane adsorption [10–13].

On the one hand, organic matters in shales are an important material condition for the formation of natural gases [14–18]. At the same time, in the process of hydrocarbon generation and evolution, organic matter will also form nanopores, providing a large number of adsorption sites for gas. The higher abundance of organic matter in shale, the stronger its adsorbability [3, 19]. The change of thermal evolution degree of organic matter not only affects the development of organic pores, but also changes the molecular structure characteristics, which is directly reflected in the adsorption capacity to shale [3, 20]. The mineral composition characteristics of shale also cannot be ignored, especially the influence of clay minerals on the adsorption of methane is very complex due to their diverse composition and the development of nanopores. Jiang et al. have found that there is a good positive correlation between methane adsorption and clay mineral content in the Chang 7 shale

of Yanchang Formation in Ordos Basin [21]. However, more studies believe that clay mineral content does not play a dominant role in the methane adsorption of shale and even has a certain negative correlation [1, 22]. The temperature and pressure environment of shale is the most important objective factor affecting the adsorption of shale [23].

From the perspective of thermodynamics, the adsorption process of natural gas is an exothermic process, while the desorption process is contrary to it. Zhang et al. established evaluation models of gas adsorption volume for different types of organic-rich shales based on Langmuir equation and thermodynamics principle of gas adsorption [7]. Ji et al. studied the adsorption thermodynamic characteristics of different types of clay minerals by the same method and pointed out that the order of gas adsorption capacity of clay minerals was smectite > illite/smectite formation > kaolinite > chlorite > illite and the adsorption heat of clay minerals is lower than that of organic matter, meaning that organic matter has a stronger gas adsorption capacity than clay minerals [4]. Li et al. pointed out that, without considering the formation water, the contribution of kerogen contained in organic-rich shale in Jiaoshiba area to the adsorption gas was less than 50%, and the contribution of kerogen in the Niutietang Formation was even less than 30% [5]. In the study of Topor et al., after removing the organic matter in shale of Silurian Baltic Basin, isothermal adsorption experiments were carried out on the mineral components [20]. And the result show that the adsorption capacity of mineral components exceeds 50% of the original shale adsorption capacity at 25 °C and 15 MPa.

Based on the previous researches, although the unit mass of gas adsorption capacity in organic matter is much higher than that of the mineral composition, however, when normalizing it to the whole shale, there is not much difference between them, and the adsorption quantity of mineral components is greater than that of organic matter, which further indicates that the adsorption quantity in shale is jointly determined by organic matter and mineral components. However, the quantitative evaluation of gas adsorption between organic matter and mineral components in shale has not been thoroughly studied at present, and the controlling effect of organic matter and inorganic mineral components on gas absorption is still not clear. In this study, taking the Niutitang Formation shale in Huijunba syncline as an example, a series of isothermal adsorption experiments were carried out on the kerogen extracted from the original shale and mineral components after H_2O_2 treatment to remove organic matter. Based on the adsorption thermodynamic principle of adsorption and combined with XRD test, organic geochemical analysis, and lower temperature physical adsorption experiment, the influence of organic matter and inorganic mineral components on methane adsorption behavior was analyzed and studied comprehensively in this area, which was to provide a deeper understanding of shale adsorption behavior process.

2. Experiments and Methods

2.1. Experiments. Three samples selected in the study were all collected from the Niutitang Formation of the YSB profile from the south wing of Huijunba syncline in the south of Hanzhong (Figure 1). The organic geochemical characteristics and mineralogical characteristics of the samples are shown in Tables 1 and 2. The organic carbon content of the original rocks ranged from 1.19% to 3.14%, and the T_{max} reached to 600 °C, indicating that the samples had reached the overmature stage and were close to the death limit of hydrocarbon generation. The mineral components are mainly composed of quartz, carbonate, rock, pyrite, feldspar, and clay minerals, in which the content of quartz reaches to 35.53%~44.37%. The content of clay minerals is lower, which is ranging from 13.81% to 16.95%. The main clay minerals are composed by illite (43%~77%) and illite/smectite formation (8%~36%), as well as a certain amount of kaolinite, chlorite, etc.

The samples were first mechanically crushed to below 20 mesh in the laboratory and then divided into three unequal parts, one of which was directly used for isothermal adsorption experiments, and the other two were performed on the extracting of kerogen and mineral components, respectively.

Kerogen extraction was completed by acid treatment. The sample with a weight about 200 g was first soaked in distilled water for about 4 hours, and then the supernatant was removed. Then, 6 mol/L hydrochloric acid was added in a water bath at 70 °C for 24 hours to fully dissolve the carbonate rock and then centrifuged to remove the supernatant. In turn, the mixed acid solution of 6 mol/L hydrochloric acid and 40%HF (2 : 3) was added and repeated this step for 3 times in 70 °C water bath for 24 h, to fully dissolve the minerals and then remove the supernatant by centrifugation. Finally, the sample was washed with distilled water to neutral and dried at 70 °C for standby application. The extractions of mineral components were treated by chemical wet oxidation. About 5 g of the samples were weighed and putted into a 200-mL beaker and then slowly added 100 mL 30% of analytically pure H_2O_2. After standing for 5 hours, the samples were heated in a water bath at 70 °C until the liquid evaporated. The process is repeated until there is no obvious reaction after adding new H_2O_2. Finally, dry the sample for standby application. To evaluate the treatment effect on samples, the TOC of all treated samples was measured once. The test results are shown in Table 1. TOC of the extracted kerogen was 20.90%~35.30%, and the samples treated with hydrogen peroxide were 0.06%~0.25%, which showed a good treatment effect.

Methane isothermal adsorption experiment was conducted on the GAI-100 high pressure isothermal adsorption apparatus produced by American Core Company, and systematic isothermal adsorption experiments were carried out on the crushed original rock samples, kerogen, and mineral components, respectively. The samples were dried at 100 °C for 24 hours until the sample weight was constant and then loaded them into the test tank. He was used as the leak detection gas to test the leakproofness of experimental system under the condition of higher than the experimental target pressure. After sample loading, leak detection, and volume calibration, the gas of 99.99% He was used for volume calibration, and 99.99% CH_4 was used

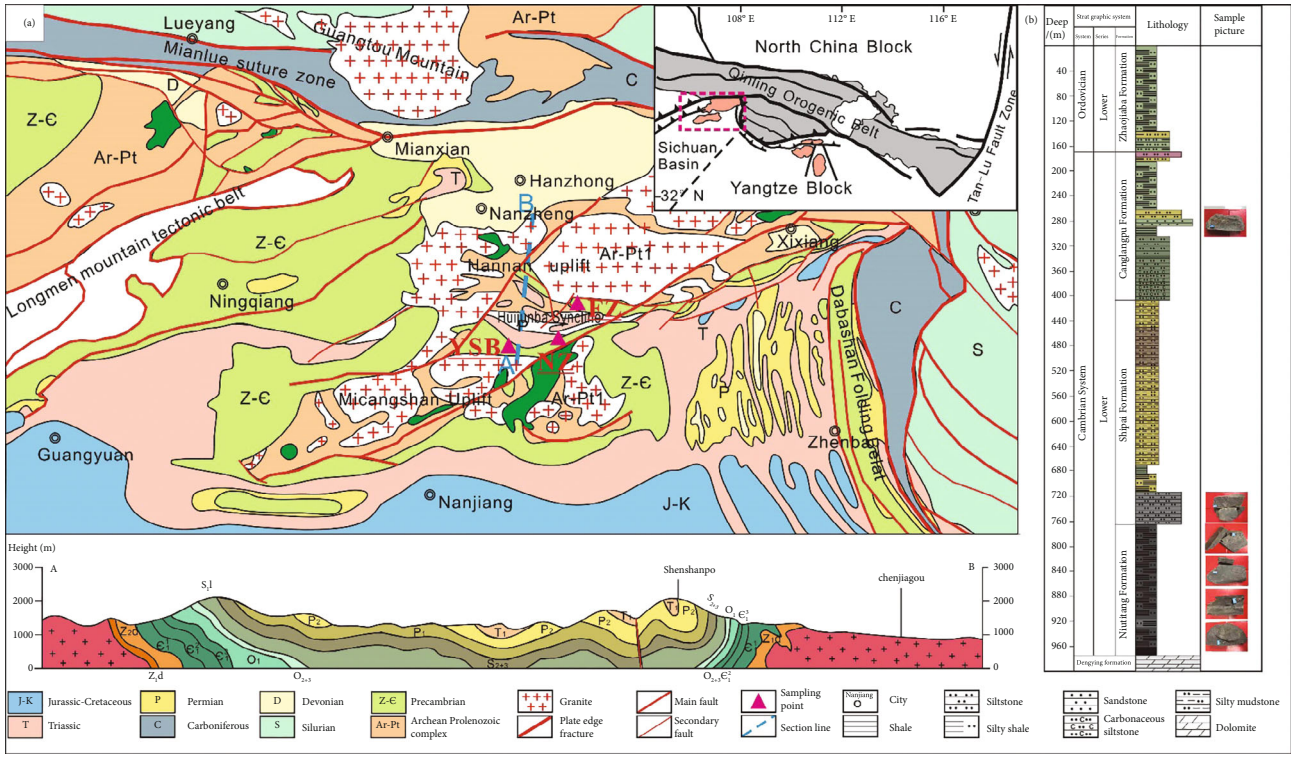

Figure 1: Sample collection point ((a) planogeologic map; (b) lithology histogram).

Table 1: Organic geochemical characteristics of the samples.

Sample	TOC %			S_1 mg/g	S_2 mg/g	S_3 mg/g	I_H mg/g	I_O mg/g	T_{max} °C
	O	K	M						
Sample 1	1.19	27.50	0.06	0.02	0.05	0.57	3	37	487
Sample 2	3.14	20.90	0.25	0.02	0.14	0.49	4	13	600
Sample 3	1.94	35.30	0.07	0.02	0.1	0.58	4	24	593

O: original rock; K: kerogen; M: mineral composition.

Table 2: Mineral composition characteristics of the samples.

Sample	Total mineral (%)					Clay minerals				
	Quartz	Carbonatite	Pyrite	Plagioclase	Potash feldspar	T	I/S	I	K	C
1	44.37	4.76	3.07	25.25	6.36	15.21	16	65	7	12
2	35.53	10.05	9.10	25.23	3.15	16.95	36	43	9	12
3	37.49	9.77	2.36	30.31	6.26	13.81	8	77	6	9

T: total content of clay minerals; I/S: illite/smectite formation; I: illite; K: kaolinite; C: chlorite.

for isothermal adsorption experiment. The maximum pressure was 13 MPa, and 12 pressure points were tested. The isothermal adsorption experiment was conducted at 35 °C, 60 °C, and 85 °C for each sample.

2.2. Methods. The adsorption of shale was tested by isothermal adsorption experiment. Then, the method of the three-dimensional Langmuir model and adsorption thermodynamics was used to calculate the standard adsorption entropy and isosteric heat of adsorption in different shales, which will be used to quantitatively evaluate the adsorption capacity of shale. Generally, the higher the adsorption heat, the stronger the adsorption capacity. The higher the adsorption entropy, the weaker the adsorption.

Langmuir isothermal adsorption model based on monolayer adsorption principle is shown in Equation (1). Assuming that the adsorbent has a uniform surface:

$$n_a = n_L \frac{KP}{1 + KP}, \tag{1}$$

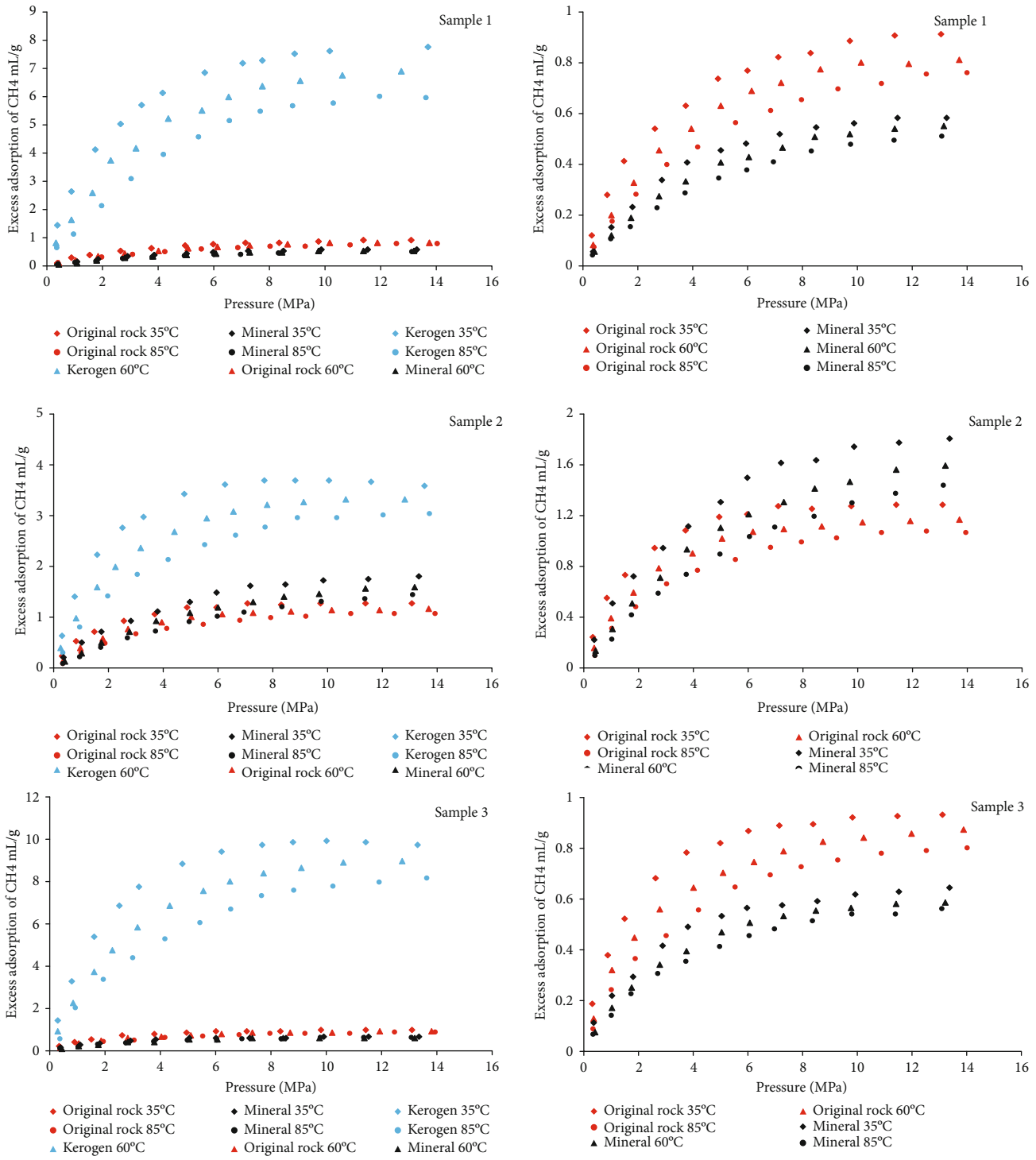

Figure 2: Excess methane adsorption capacity of each sample obtained from the experiment.

where n_a is the absolute methane adsorption capacity, mL/g; n_L is the Langmuir maximum adsorption capacity on the surface of adsorbent, mL/g; K is the Langmuir constant, 1/MPa; and P is the pressure, MPa.

For the assumed conditions of Langmuir, adsorption model are only applicable under the condition of lower pressure. Under the condition of higher pressure, the increasing density of gaseous methane makes this assumption inapplicable for the conditions with large error. Therefore, the Langmuir model in Equation (2) of excess adsorption capacity is introduced to deduct the influence of adsorption phase volume on this model under the condition of supercritical pressure:

$$n_e = n_L \frac{KP}{1+KP}\left(1-\frac{\rho_g}{\rho_a}\right), \tag{2}$$

Table 3: Isothermal adsorption data.

Sample 1		Sample 2		Sample 3		Kerogen 1		Kerogen 2		Kerogen 3		Mineral 1		Mineral 2		Mineral 3	
		35 °C						35 °C						35 °C			
P/MPa	V/mL/g	P/MPa	V/mL/g	P/MPa	V/mL/g	P/MPa	V/mL/g	P/MPa	V/mL/g	P/MPa	V/mL/g	P/MPa	V/mL/g	P/MPa	V/mL/g	P/MPa	V/mL/g
0.33	0.12	0.32	0.25	0.34	0.19	0.33	1.43	0.31	0.75	0.29	1.65	0.35	0.1	0.38	0.23	0.39	0.11
0.86	0.28	0.84	0.55	0.88	0.38	0.85	2.64	0.81	1.45	0.78	3.33	1.04	0.21	1.04	0.51	1.07	0.22
1.5	0.41	1.48	0.74	1.52	0.52	1.69	4.13	1.62	2.17	1.59	5.12	1.78	0.31	1.78	0.73	1.81	0.3
2.6	0.54	2.58	0.95	2.64	0.68	2.6	5.01	2.52	2.73	2.49	6.56	2.86	0.41	2.86	0.95	2.9	0.42
3.72	0.64	3.71	1.09	3.77	0.78	3.35	5.72	3.28	2.99	3.25	7.25	3.81	0.46	3.81	1.12	3.84	0.49
4.92	0.74	4.91	1.2	4.97	0.82	4.13	6.19	4.81	3.28	4.78	8.45	5	0.54	4.99	1.31	5.04	0.53
5.97	0.77	5.97	1.22	6.02	0.87	5.62	6.9	6.25	3.53	6.22	9.18	5.96	0.58	5.95	1.5	6	0.56
7.09	0.83	7.1	1.28	7.15	0.89	6.98	7.23	7.68	3.6	7.67	9.18	7.18	0.58	7.18	1.62	7.24	0.58
8.31	0.84	8.32	1.26	8.38	0.89	7.71	7.33	8.81	3.62	8.8	9.41	8.48	0.62	8.49	1.65	8.54	0.59
9.74	0.89	9.75	1.28	9.82	0.92	8.88	7.57	10.06	3.66	10.05	9.72	9.85	0.64	9.86	1.74	9.91	0.62
11.36	0.91	11.38	1.29	11.45	0.93	10.15	7.67	11.58	3.7	11.46	9.84	11.47	0.65	11.49	1.78	11.54	0.63
13.04	0.92	13.06	1.29	13.11	0.93	13.67	7.78	13.53	3.74	13.34	9.91	13.27	0.65	13.33	1.81	13.38	0.65
		60 °C						60 °C						60 °C			
P/MPa	V/mL/g	P/MPa	V/mL/g	P/MPa	V/mL/g	P/MPa	V/mL/g	P/MPa	V/mL/g	P/MPa	V/mL/g	P/MPa	V/mL/g	P/MPa	V/mL/g	P/MPa	V/mL/g
0.38	0.08	0.36	0.16	0.38	0.13	0.3	0.81	0.3	0.56	0.28	1.15	0.42	0.09	0.41	0.14	0.42	0.06
1.02	0.2	1	0.4	1.04	0.32	0.83	1.62	0.84	0.99	0.82	2.7	1.04	0.16	1.02	0.31	1.06	0.17
1.82	0.33	1.81	0.6	1.86	0.45	1.59	2.59	1.62	1.78	1.58	4.08	1.75	0.24	1.73	0.51	1.77	0.25
2.75	0.45	2.74	0.79	2.8	0.56	2.26	3.72	2.29	2	2.26	4.9	2.78	0.33	2.76	0.72	2.81	0.34
3.95	0.54	3.96	0.9	4.01	0.64	3.16	4.18	3.2	2.41	3.17	5.68	3.75	0.41	3.74	0.94	3.79	0.4
5.03	0.63	5.05	1.02	5.1	0.7	4.35	5.22	4.4	2.7	4.36	6.57	5	0.47	4.98	1.11	5.04	0.47
6.12	0.69	6.16	1.08	6.22	0.74	5.53	5.49	5.6	2.9	5.55	7.32	6.03	0.53	6.02	1.22	6.06	0.51
7.23	0.73	7.27	1.1	7.32	0.79	6.49	6.03	6.59	3.07	6.54	7.84	7.27	0.54	7.27	1.31	7.32	0.53
8.63	0.78	8.67	1.12	8.72	0.82	7.71	6.41	7.8	3.22	7.75	8.43	8.43	0.58	8.43	1.42	8.47	0.55
10.12	0.81	10.15	1.15	10.22	0.84	9.06	6.6	9.15	3.31	9.1	8.82	9.71	0.6	9.71	1.47	9.76	0.56
11.85	0.8	11.9	1.17	11.96	0.86	10.59	6.79	10.69	3.41	10.64	9.09	11.36	0.61	11.38	1.57	11.42	0.58
13.73	0.82	13.72	1.17	13.86	0.87	12.7	6.93	12.81	3.46	12.77	9.13	13.17	0.61	13.18	1.6	13.23	0.58
		85 °C						85 °C						85 °C			
P/MPa	V/mL/g	P/MPa	V/mL/g	P/MPa	V/mL/g	P/MPa	V/mL/g	P/MPa	V/mL/g	P/MPa	V/mL/g	P/MPa	V/mL/g	P/MPa	V/mL/g	P/MPa	V/mL/g
0.42	0.07	0.39	0.1	0.4	0.09	0.37	0.65	0.38	0.31	0.36	0.5	0.39	0.08	0.39	0.1	0.39	0.06
1.07	0.17	1.02	0.31	1.05	0.24	0.95	1.12	0.97	0.8	0.93	1.93	1.02	0.14	1.01	0.23	1.03	0.14
1.95	0.28	1.89	0.48	1.93	0.36	1.96	2.1	2	1.41	1.95	3.3	1.76	0.2	1.76	0.42	1.77	0.22
3.08	0.4	3.02	0.67	3.07	0.45	3.03	3.08	3.08	1.85	3.03	4.34	2.72	0.29	2.73	0.59	2.75	0.3
4.22	0.46	4.17	0.77	4.21	0.55	4.18	3.92	4.24	2.14	4.19	5.21	3.75	0.34	3.77	0.74	3.79	0.35
5.56	0.56	5.52	0.85	5.56	0.65	5.45	4.57	5.54	2.44	5.47	6.01	4.95	0.41	4.98	0.9	5	0.41
6.87	0.61	6.82	0.95	6.87	0.69	6.57	5.12	6.66	2.61	6.59	6.64	6	0.46	6.03	1.03	6.06	0.45
7.99	0.66	7.95	0.99	7.99	0.72	7.66	5.45	7.75	2.78	7.68	7.27	6.94	0.49	6.98	1.11	7	0.48
9.29	0.7	9.25	1.03	9.29	0.75	8.81	5.63	8.91	2.95	8.84	7.51	8.32	0.53	8.39	1.2	8.41	0.51
10.91	0.72	10.86	1.06	10.9	0.77	10.25	5.76	10.37	2.95	10.29	7.73	9.78	0.54	9.82	1.31	9.84	0.54
12.54	0.76	12.49	1.08	12.53	0.79	11.93	6.03	12.06	3.02	11.98	7.93	11.37	0.58	11.4	1.37	11.41	0.53
14.02	0.76	13.98	1.07	14.01	0.8	13.62	6	13.75	3.05	13.67	8.08	13.09	0.59	13.12	1.44	13.12	0.56

Table 4: Langmuir constant, maximal adsorption capacity n_{max} and thermodynamic parameters.

T/°C	Sample 1		Sample 2		Sample 3	
	Original rock		Original rock		Original rock	
	n_L	K	n_L	K	n_L	K
35	1.543	0.224	1.895	0.445	1.372	0.41
60	1.529	0.158	1.845	0.282	1.362	0.262
85	1.518	0.118	1.819	0.196	1.361	0.184
	q*	ΔS^0*	q	ΔS^0	q	ΔS^0
	12.05	-70.64	15.10	-74.89	14.59	-74.01
	Kerogen		Kerogen		Kerogen	
	n_L	K	n_L	K	n_L	K
35	12.264	0.214	5.504	0.434	15.257	0.349
60	12.154	0.151	5.321	0.275	15.188	0.211
85	12.104	0.111	5.243	0.186	15.114	0.142
	q	ΔS^0	q	ΔS^0	q	ΔS^0
	16.09	-81.39	15.09	-75.16	14.98	-77.03
	Mineral		Mineral		Mineral	
	n_L	K	n_L	K	n_L	K
35	1.106	0.161	3.604	0.14	1.067	0.236
60	1.124	0.122	3.361	0.117	1.013	0.194
85	1.118	0.097	3.197	0.095	0.995	0.161
	q	ΔS^0	q	ΔS^0	q	ΔS^0
	8.80	-60.65	11.40	-72.22	7.06	-54.11

where n_e is the excess adsorption capacity, ρ_g is the density of methane at experimental temperature (K) and pressure (MPa), and ρ_a is the density of adsorbed methane, which is generally equal to 424 mg/mL (the density of liquid methane at its boiling point under standard atmospheric pressure) [6]. Langmuir constant K is a function of temperature (K):

$$\ln K = \frac{q}{RT} + \frac{\Delta s^0}{R} - \ln p^0, \tag{3}$$

where q is the isosteric heat of adsorption, kJ mol^{-1}; $\Delta_S{}^0$ is the standard adsorption entropy J mol^{-1} K^{-1}; p^0 is the standard atmospheric pressure, and R is the gas constant, 8.314 J mol^{-1} K^{-1}.

According to the results of isothermal adsorption experiments at different temperatures, the Langmuir constant can be obtained by using the least square method, and the parameters of methane adsorption thermodynamic can be obtained by using Equation (3). Based on this, the content of adsorption gas in shale under different temperatures and pressure can be calculated back.

3. Experimental Results

3.1. Isothermal Adsorption Characteristics. Figure 2 and Table 3 show the excess methane adsorption capacity of each sample obtained from the experiment, which is similar to a large number of previous researches [4, 6, 7, 24]. During the experiment, the excess methane adsorption capacity of the sample increased rapidly firstly with increasing pressure and then gradually tended to be stable after a certain pressure. With the increasing temperature, the adsorption capacity under the corresponding pressure decreased accordingly. The methane adsorption capacity of the three samples was significantly higher than that of the corresponding original rocks and minerals. Among them, the methane adsorption capacity of samples 1 and 3 was slightly higher than that of minerals, while the methane adsorption capacity of sample 2 was higher than that of minerals at the lower pressure stage. When the pressure was higher than 4 MPa, the mineral adsorption capacity began to be higher than that of original rock.

3.2. Three-Dimensional Langmuir Fitting and Adsorption Thermodynamic Parameters. This study was based on the three-dimensional Langmuir model and combined with the isothermal adsorption experiments together. The Langmuir constant and maximum adsorption capacity (n_{max}) calculated in these series of experiments are presented in Table 4. The adsorption thermodynamics parameter obtained by the linear relationship between ln (K) and 1/T (inverse of Kelvin temperature) in Figure 3 is also shown in Table 4.

The isosteric heat of adsorption in original rocks is closed to that in kerogen of sample 2. Different situation occurs in samples 1 and 3, which showed that the equal heat of adsorption in kerogen was the highest, but the standard adsorption entropy was the lowest, while the equal heat of adsorption of mineral components was the lowest, but the standard adsorption entropy was the highest. These results prove that kerogen has the strongest adsorption and mineral components have poor adsorption from the thermodynamic perspective. In Figure 4, the comparisons between thermodynamic parameters obtained in this study are almost same to those in previous studies. Thermodynamic adsorptions of mineral components are similar to those of clay minerals given by Ji et al. [4]. The adsorption property of kerogen is between type I and type II kerogen given by Zhang et al. [7]. The sample in the study belongs to a typical marine sedimentary shale, and the kerogen is mainly Type I [25, 26], and the main reason for this difference is the higher maturity [26]. A large amount of adsorption potentials are formed after the aromatization of organic matter, which makes its adsorbability is higher than that of type I kerogen. The adsorption of shale is close to that of North American shale obtained by Zhang et al. and Gasparik et al., but much lower than that of Longmaxi Formation and Wufeng Formation shale in Sichuan Basin [5, 7, 24, 27].

4. Discussion

4.1. The Adsorption Capacity of Shale under Geological Conditions. After Langmuir adsorption, thermodynamic parameters are determined; Langmuir constant, formation temperature, formation pressure, Langmuir maximum adsorption capacity, and other parameters are functions of strata depth (Figure 5(a)). Assume that the geothermal gradient is 3°C/100 m and the pressure gradient is 1 MPa/

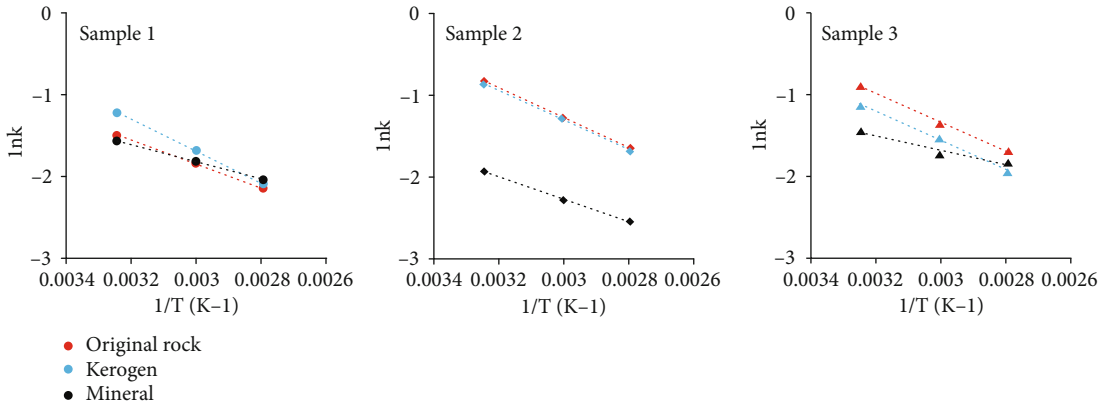

Figure 3: The adsorption thermodynamics parameter obtained by the linear relationship between ln (K) and 1/T (inverse of Kelvin temperature).

100 m in this area, and then based on the parameters listed in Table 4, the absolute and excess adsorption capacity of methane under geological conditions at different burial depths can be calculated by three dimensional Langmuir method (Equations (1), (2), and (3)).

The simulation results are shown in Figure 6, for the effect of formation water and other gas components on methane adsorption was not considered during the experiment, so the maximum adsorption amount of shale under geological conditions is obtained. It is also seen from the figure that, with the increasing depth, the absolute and excess adsorption capacity do not increase along with it together, but appear a maximum after reaching a certain depth, and then decrease gradually. In addition, it can be seen that the excess adsorption amount by volume correction is significantly lower than the absolute adsorption amount after 300 m, which has an important impact on the potential evaluation of resources. While when the in situ gas content of shale is calculated without considering the adsorbed gas volume, the corresponding resource evaluation amount will be significantly larger. When the burial depth ranges in 450 m~900 m, the excess adsorption capacity reaches to the highest, and the average maximum excess adsorption capacity is 1.01 mL/g. When the burial depth reaches to 3000 m, the average excess adsorption capacity decreases to 0.79 mL/g with the reduction rate of 21.8%.

4.2. Contribution of Organic Matter and Mineral Components to Shale Adsorption Capacity

4.2.1. Adsorption Capacity of Organic Matter and Mineral Components. The calculation method is the same as that of original rock; we calculated the corresponding adsorption gas content of kerogen and mineral components separately. The relationship between the maximum adsorption capacity of kerogen and mineral components and temperature is shown in Figures 5(b) and 5(c). Based on this, the adsorption capacity of kerogen and minerals under geological conditions can be deduced by combining with adsorption thermodynamic parameters.

In Figure 7, the tendency of methane adsorption in kerogen with depth is slightly different to that in the original rock, which is mainly reflected in the absolute adsorption capacity. The absolute adsorption amount increases rapidly with the increasing depth and keeps stable gradually after 500 m, while the excess adsorption rises rapidly in shallow and decreased gradually after the maximum at about 600 m~900 m. In addition, the decelerated value is slightly lower than that in the original rock. The average maximum excess adsorption is 6.76 mL/g, which is corresponding to a depth of 900 m. When the depth reaches to 3000 m, the excess adsorption is reduced to 5.29 mL/g with a reduction ratio of 21.7%, which is similar to the reduction rate in the original rock.

The variation of methane adsorption of minerals with depth (Figure 8) is similar to that of the original rock sample. In terms of adsorption capacity, the excess adsorption capacity increases rapidly with the increasing depth and then gradually tends to be stable at about 500 m, reaching the maximum at 1200 m, and then gradually decreases. The average maximum excess adsorption capacity was 0.96 mL/g; when the depth was 3000 m, the average excess adsorption capacity was reduced to 0.84 mL/g with a reduction ratio of 12.5%, 9.3%, and 9.2%, which is lower than that of protolith and kerogen, respectively.

4.2.2. Contribution of Organic Matter and Mineral Components to the Adsorption Capacity. To clarify the contribution of organic matter and mineral components to the adsorption capacity in shale, we normalized the organic matter before and after sample treatment based on the law of conservation of matter (Equation (4)). And then the adsorption capacity per unit of organic matter is obtained, and the corresponding contribution ratio of organic matter to adsorption capacity could also be gained further:

$$R_{no} = \frac{K_n}{K_{TOC}} \times R_{TOC}, \tag{4}$$

where R_{no} is the excess adsorption of organic matter in shale, K_n is the excess adsorption of organic matter in kerogen, K_{TOC} is the total organic matter content in kerogen, and R_{TOC} is the total organic matter in shale.

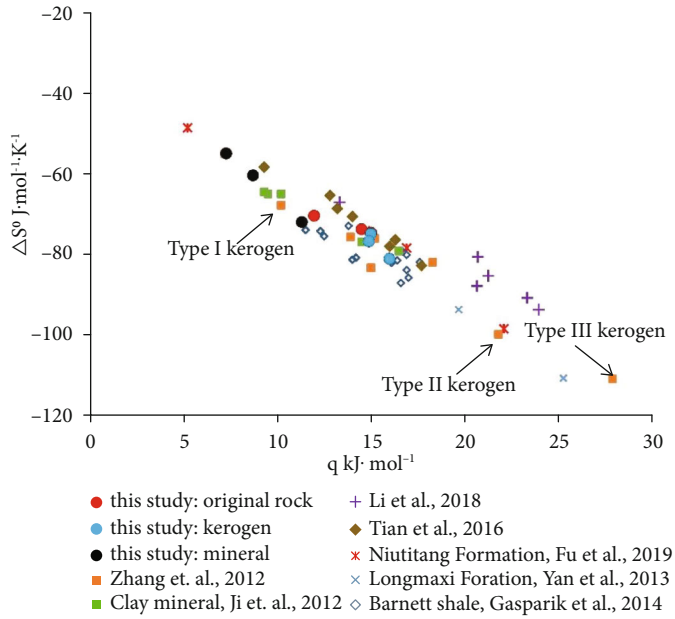

Figure 4: The thermodynamic parameters obtained in different adsorbents.

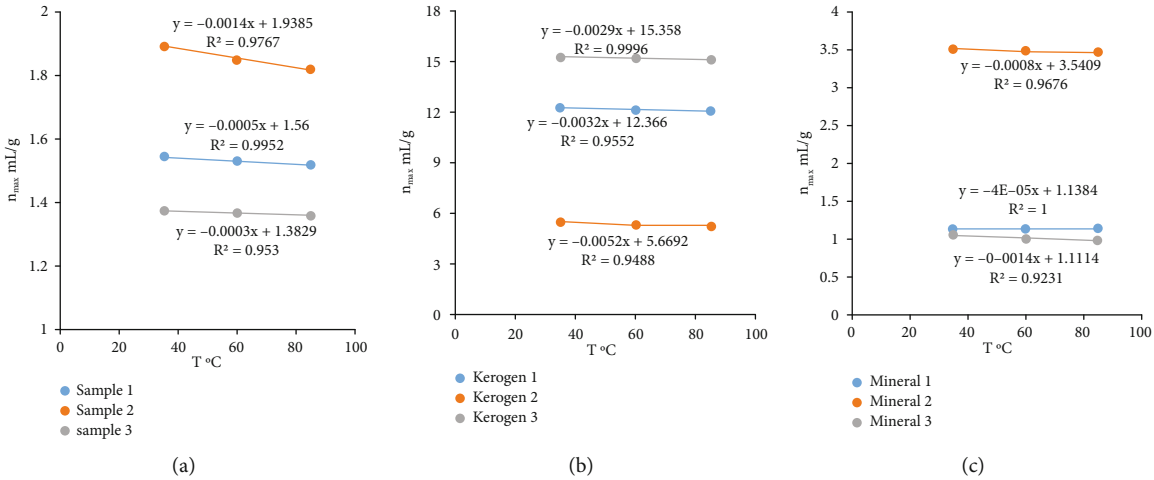

Figure 5: The relationships between Langmuir maximum adsorption capacity of shale (a), kerogen (b), mineral compositions (c), and temperatures.

Similarly, in the minerals, clay minerals play a decisive effect on the adsorption of methane, and the effects by other minerals could be relatively negligible. Therefore, by the unit normalized calculation of clay mineral in the adsorption quantity of mineral components, combining with the proportion of clay minerals (Equation (5)), we could get the contribution of mineral components to the total amount of shale adsorption:

$$R_{nm} = \frac{M_n}{M_{CLAY}} \times R_{CLAY,} \tag{5}$$

where R_{nm} is the excess adsorption of mineral composition in shale, M_n is the excess adsorption of mineral composition, M_{CALY} is the content of clay mineral in total mineral components, and R_{CALY} is the content of clay mineral in shale.

The adsorption amount of organic matter and its contribution to the total adsorption changing with depth are shown in Figure 9. The proportion of organic matter adsorption to the total adsorption first decreases rapidly with the increasing depth and then becomes stably exceeds about 900 m. The adsorption capacity of organic matter in shale can reach to 0.31~0.54 mL/g, and the corresponding proportion of total adsorption capacity is 33.2 ~ 48.7%. The average adsorption capacity is 0.45 mL/g, and the average proportion is 38.9%. When the burial depth of shale reaches to 3000 m, the adsorption capacity of organic matter is 0.24~0.41 mL/g, which accounts for 29.3~46.7% of the total adsorption capacity, and the corresponding average adsorption capacity and proportion were 0.35 mL/g and 35.2%, respectively, on average. This result is slightly lower than that calculated for Wufeng-Longmaxi Formation shale in the Jiaoshiba area

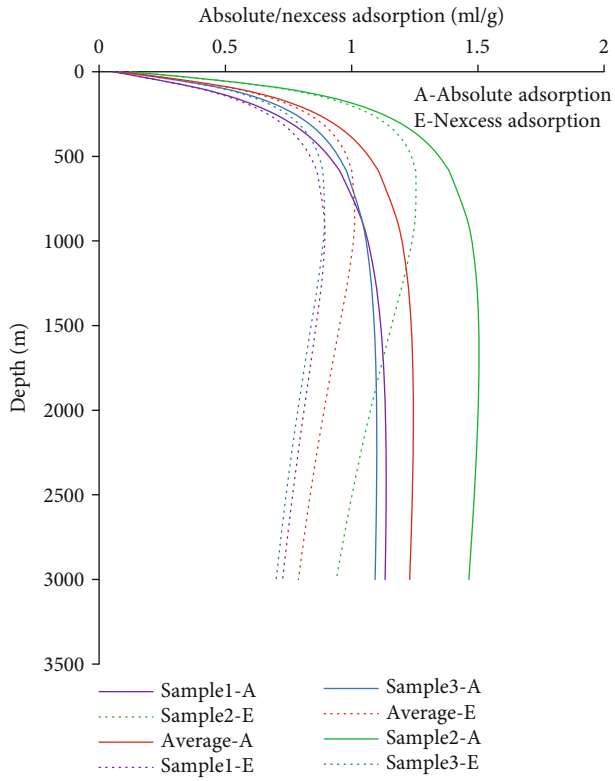

Figure 6: Methane adsorption capacity of original rocks in three samples under geological conditions.

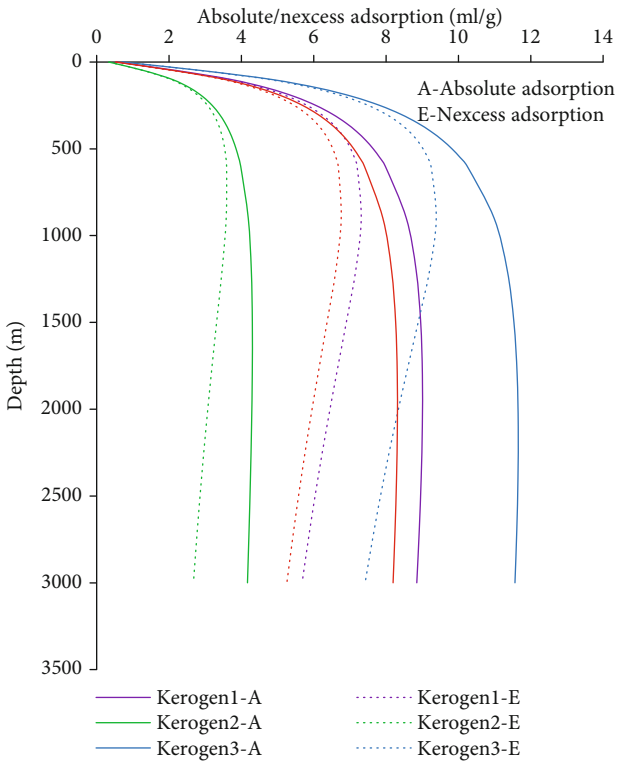

Figure 7: Methane adsorption capacity of kerogen in three samples under geological conditions.

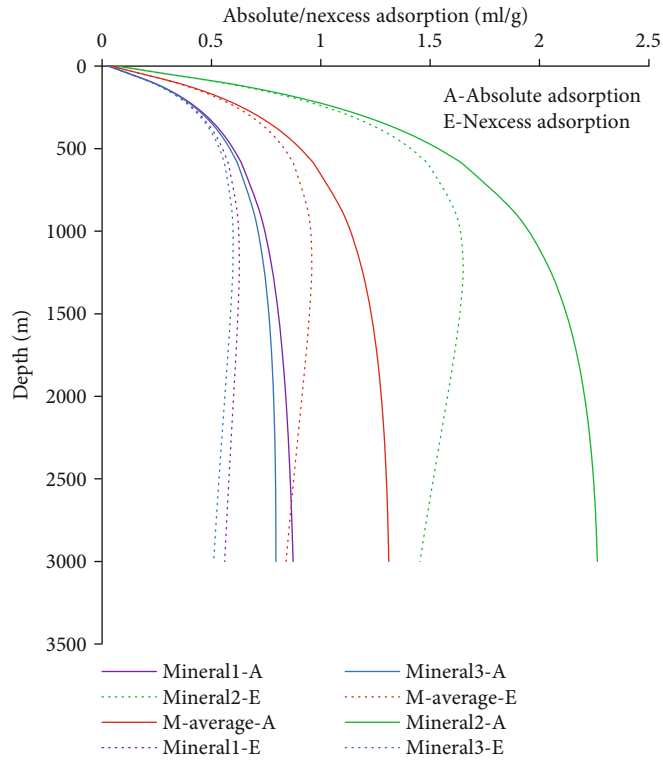

Figure 8: Methane adsorption capacity of mineral composition in three samples under geological conditions.

[5]. The adsorption properties of kerogen reflected by the thermodynamic parameters obtained in this study are slightly worse than that in the Wufeng-Longmaxi Formation shale in the Jiaoshiba area, which is consistent with the calculated results.

The adsorption amount of mineral component and its contribution to the total adsorption amount changing with depth in shale are shown in Figure 10. For the incomplete removal of organic matter in the three samples, there is still part of residual organic matter occurring in the samples (Table 1). Among them, the highest content of residual organic matter occurred in sample 2, with the residual TOC = 0.25%. Besides, the calculated proportion of mineral components to adsorption is higher than the adsorption amount of original rock at 2400 m, which is unreasonable. For the residual organic matter may be one of the direct causes to the result, we will not discuss the adsorption capacity of mineral components in sample 2 in the following section. On the other hand, due to the hydrophilic characteristics of clay minerals, the existence of formation water will greatly limit the adsorption capacity of mineral components to methane, which will result in the lower contribution of mineral components to the methane adsorption capacity under the actual geological conditions. Therefore, the adsorption proportion of mineral components obtained from these results can only be the maximum proportion under the geological conditions.

The proportion of mineral components to the total adsorption capacity of shale increases rapidly first with the

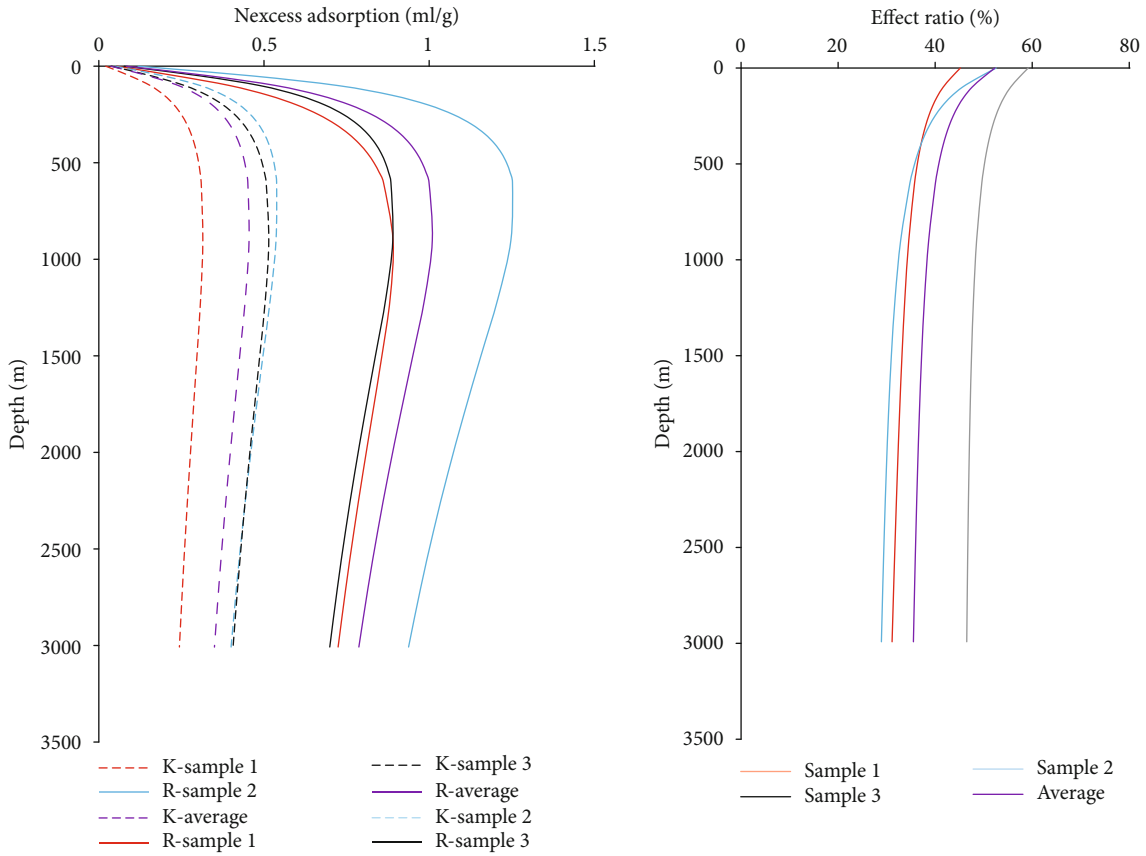

Figure 9: The adsorption amount of organic matte and its contribution to the total adsorption amount changing with depth in shale.

increasing depth, which is opposite to the situation of organic matter. When the burial depth of shale exceeds about 900 m, the adsorption capacity of mineral components gradually tends to be stable. The adsorption capacity of mineral components in shale can reach up to 0.54~0.59 mL/g with the corresponding proportion of 60.99~61.4% to the total adsorption capacity. And the corresponding average adsorption capacity and proportion was 0.57 mL/g and 63.5%, respectively, on average. When the burial depth of shale reaches 3000 m, the adsorption capacity of mineral components is 0.47-0.54 mL/g, which accounts for the total adsorption capacity with 66.4~73.6%.

4.3. Influence Mechanism of Methane Adsorption under Organic-Inorganic Interaction of Shale. The essence of methane adsorption in shale is, under a certain temperature and pressure, as well as with the acting force between microscopic pore surface and methane molecules, making the free methane molecules bounded to the pore surface and turned into the adsorbed state, which is accompanied by both the exothermic process of adsorption and endothermic process. And when the adsorption is in equilibrium, the adsorbed heat release and desorbed caloric receptivity maintain a dynamic balance [7]. Therefore, the most direct factor to the adsorbability of shale is the changing pore characters in the adsorbents. Specifically, pore characters include two aspects: pore type and pore structure. Pore type determines the adsorption amount per unit area of pore surface, and then the pore structure determines the total adsorption amount of shale.

For the decisive effect of different pore types occurring on the adsorption capacity of the adsorbent pore surface, there is a better ability of organic matter to absorb methane. Because organic pores are rich in aromatic molecular functional groups, they are more likely to form a variety of forces with methane molecules or even form hydrogen bonds, including dispersion forces, induction forces, van der Waals forces, and even hydrogen bonds, so they have a stronger adsorption capacity for methane. However, the interaction between mineral pores and methane molecules is mainly affected by the van der Waals force, which is weaker, so the adsorption capacity of methane on the mineral pore surface is weaker than that of organic pores.

Pore structure directly affects the total amount of methane adsorption in shale. When the specific surface area of pores is same, the stronger of the adsorption ability is, the higher of the total amount adsorption will be. The diameter of methane molecular dynamics is 0.38 nm, that is to say, when the pore diameter is less than 0.38 nm, methane molecules cannot enter into the pores as well as adsorb. In general, after the maturity of organic matter reaches to a certain value, more developed micropores and higher specific surface area will occur. In addition, the micropores are the most developed in clay minerals compared to other mineral components, which could also provide a lot of adsorption potential to methane in shale.

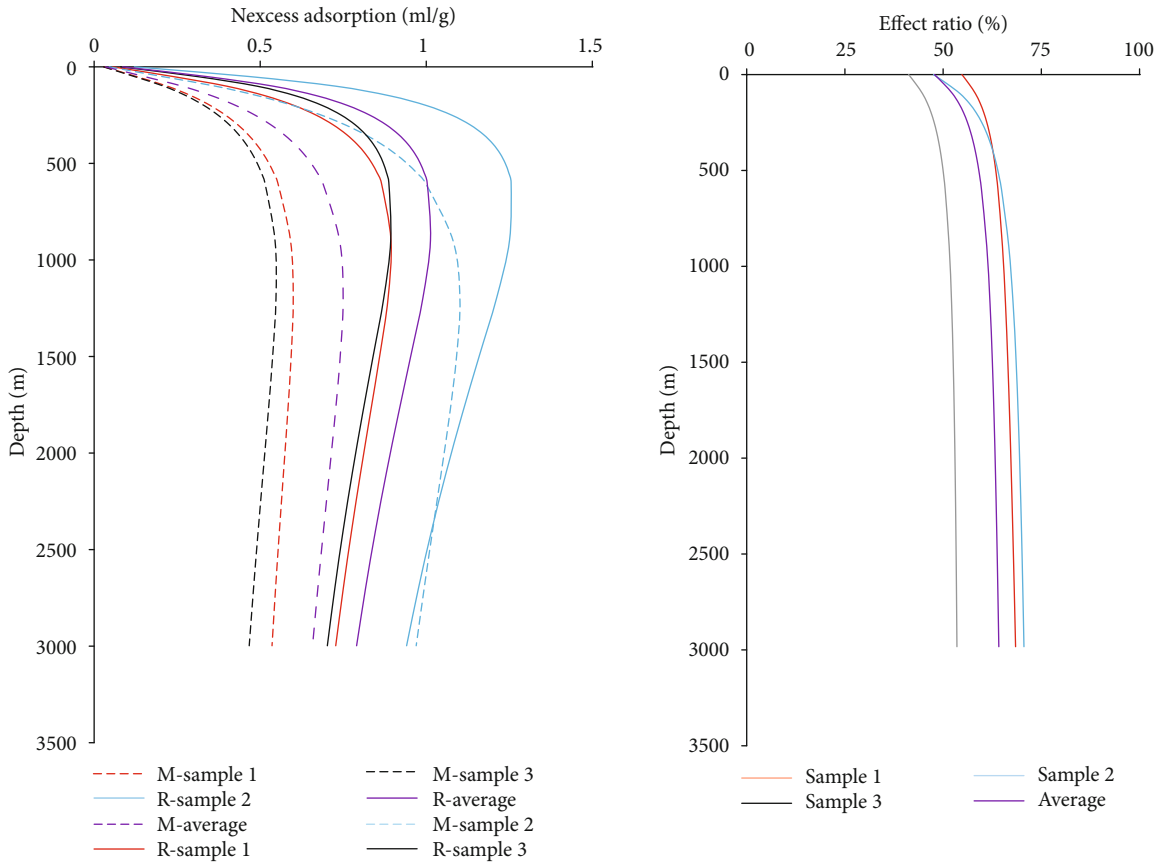

Figure 10: The adsorption amount of mineral composition and its contribution to the total adsorption amount changing with depth in shale.

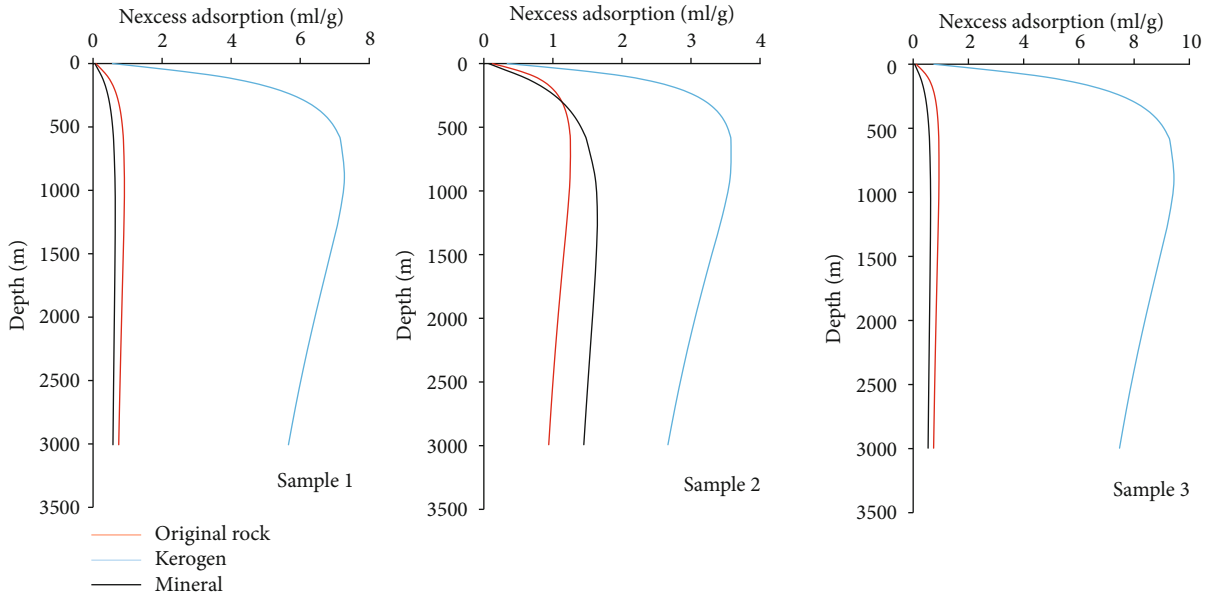

Figure 11: The adsorption capacity of the original rock, kerogen, and mineral composition in three sample under geological conditions.

4.3.1. Constraints of Pore Structure on Adsorbability. By comparing the adsorption capacity of the original rock and each single component of the sample under geological conditions (Figure 11), the adsorption capacity per unit of organic matter is the highest, while the adsorption capacity is the lowest in the mineral constituent when the organic matter removal degree is the highest. However, due to the slightly higher residual organic matter content in sample 2,

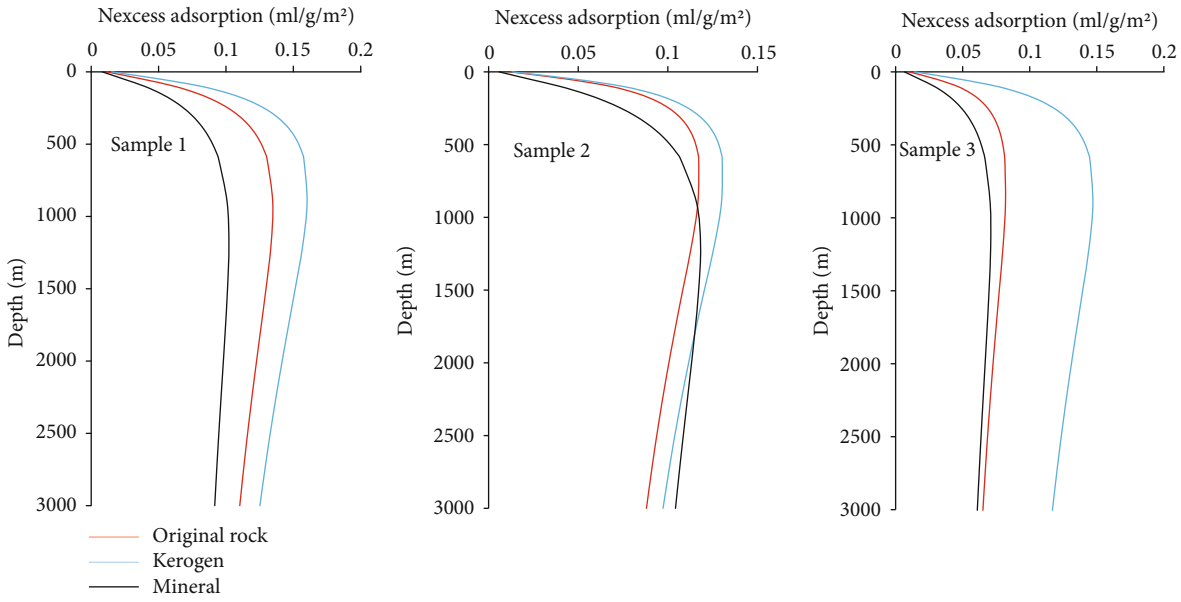

Figure 12: The adsorption capacity per unit surface area of the original rock, kerogen, and mineral composition in three sample.

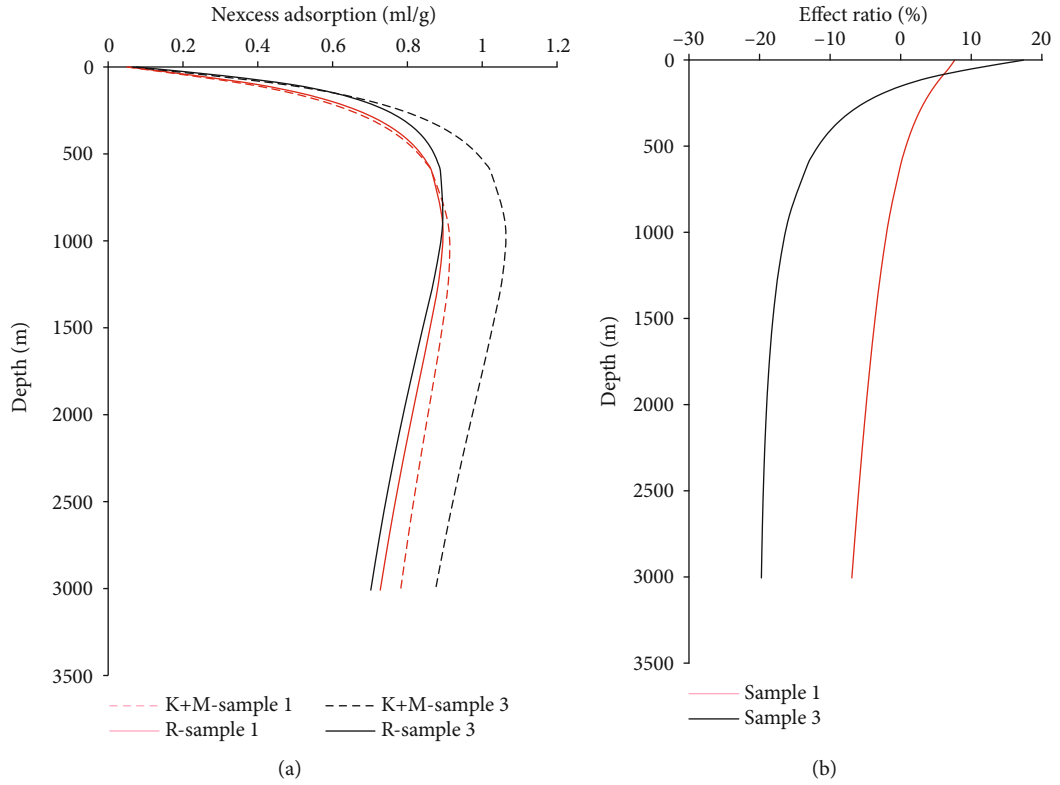

Figure 13: The comparison between calculated total organic-inorganic adsorption with the actual fitting adsorption of original rock.

which may affect the calculation results, and then making the recovery results under geological conditions show that the adsorption capacity of mineral and kerogen are higher than that of the original rock when the buried depth exceeds 300 m. However, this result can only reflect the adsorption capacity per unit mass, but not enough to reflect the relevant information about the methane adsorption capacity on the adsorbent surface.

To clarify the relationship between the adsorption capacity and the composition difference in three samples, the results of previous studies on the pore structure of original rock, kerogen, organic matter, and minerals were used to unify the above calculation results on the specific surface area of the adsorbent for comparison, to obtain deeper information in this study. In Figure 12, after the adsorption ability of three samples unified to the pore surface, the better efficiency of organic matter

removal in samples 1 and 3 and their highest and lowest adsorption capacity per unit surface area occur in kerogen and minerals, respectively. However, for sample 2, this characteristic only appears at the shallow level less than 1000 m, which possibly due to the influence of residual organic matter.

For samples 1 and 3 (Figure 12), the adsorption thermodynamic parameters of organic matter and mineral components of both (Table 4) are consistent with the adsorption characteristics per unit specific surface area. Both of them show that the adsorption capacity per unit specific surface area is lower when the adsorption heat is low. However, the relationship between the adsorption thermodynamic parameters and the specific surface area of original rocks is different, while the reasons for this need to be further studied. Our previous study on the development mechanism of pore structure found that the sum of specific surface area and pore volume of organic-inorganic pores calculated by the method of weighting were greater than that in the actual original rock. However, in terms of specific surface area, the increased proportion is 18.7% in sample 1, and that only is 3.5% in sample 3, which may reflect the great difference in pore development between them.

Especially in terms of the organic-inorganic marginal pores, the development proportion may be lower in sample 1, that is to say, the area of organic pores sealed by mineral components in sample 1 may be larger and further leads to the reduction of the effective adsorption area in the original rock. As a result, although the adsorption thermodynamic parameters show the good adsorptivity in sample 1, the adsorption per unit area is lower than that of sample 3.

4.3.2. Influence of the Organic-Inorganic Composition Difference on the Adsorption in Shale. It is very difficult to quantitatively study the contribution ratio of organic matter and mineral components to methane adsorption in shale. In the study on the contribution proportion of organic-inorganic adsorption to shale adsorption mentioned above, we, respectively, obtained the amount of organic-inorganic adsorption in shale. Along this way of thinking, we compared the calculated value based on the total amount of organic-inorganic single component adsorption in shale with the actual fitting adsorption of the original rock. Since organic matter has a great influence on the total amount of adsorption in the mineral component of sample 2, we only discuss the corresponding influences about samples 1 and sample 3 (Figure 13(a)). It can be seen that when the burial depth reaches a certain value (sample 1: 600 m; sample 3: 150 m), the fitting excess adsorption amount of the actual shale is lower than the sum of treated kerogen and mineral, while the fitting result of the actual shale is higher than the calculated result of treated single component when the burial depth is relatively shallow.

Here, we refer to the difference between the organic-inorganic calculated results and the actual fitting results as the influence rate (∂, Equation (6)) of diagenesis on the adsorption of a single component:

$$\partial = \frac{N_R - N_{K+M}}{N_R} \times 100\%, \tag{6}$$

where N_R is the actual fitting excess adsorption in original rock and N_{K+M} is the sum of calculated organic-inorganic excess adsorption based on the kerogen and mineral composition (Figure 13(b)). It shows that when the burial depth is relatively shallow, the $\partial > 0$, that is to say, the actual fitting value is greater than the organic-inorganic calculated value; diagenesis has a promoting effect on the total adsorption. And with the increasing depth, the ∂ will gradually reduce to below 0, that is to say, when the critical depth is reached, diagenesis has an inhibiting effect on the total adsorption. Within the depth range in this study, the ∂ varied from −6.9~7.7% (sample 1) to −19.7~17.4% (sample 3), respectively.

5. Conclusion

Based on the three-dimensional Langmuir model to get the excess adsorption of Niutitang Formation shale in Huijunba, synclinal reaches the highest value when the burial depth is about 450-900 m, and the average maximum excess adsorption is 1.01 ml/g. However, its average excess adsorption decreases to 0.79 ml/g when the burial depth reaches to 3000 m. For kerogen, its maximum average excess adsorption is 6.76 ml/g corresponding to a depth of 900 m, but decreases to 5.29 ml/g when the depth reaches to 3000 m. For mineral components, the maximum average excess adsorption is 0.96 ml/g, but decreases to 0.84 ml/g when the depth reaches to 3000 m.

The primary factor affecting the adsorbability is the complex changing pore characteristics caused by the heterogeneity in shale. This is mainly reflected in that the pore type determines the gas adsorption per unit area of the pore surface, while the pore structure determines the total adsorption in shale. Compared with the adsorption capacity of organic matter and mineral components, the diagenesis can promote the total adsorption when the burial depth is relatively shallow, and the diagenesis will change to inhibit the total adsorption with the increasing depth. When the burial depth reaches to 3000 m under geological conditions, the adsorption of organic matter in shale is 0.24~0.41 mL/g, accounting for 29.3%~46.7% of the total adsorption, while the adsorption of mineral components can reach to 0.47~0.54 mL/g, accounting for 66.4%~73.6% of the total adsorption.

Data Availability

The picture or tabular data used to support the findings of this study are included within the article.

Conflicts of Interest

The authors declare that they have no conflicts of interest.

Acknowledgments

This research was supported by the National Natural Science Foundation of China (Grant Number: 41903060), the Natural Science Foundation of Shaanxi Province (2021JQ-953, 2021JLM-14, 2020JQ-1000, and 2019JQ-996), Post-doctoral

Foundation of Shaanxi Province (2018BSHQYXMZZ07), and the Open Foundation of Top Disciplines in Yangtze University (2019KFJJ0818019).

References

[1] M. Gasparik, P. Bertier, Y. Gensterblum, A. Ghanizadeh, B. M. Krooss, and R. Littke, "Geological controls on the methane storage capacity in organic-rich shales," *International Journal of Coal Geology*, vol. 123, pp. 34–51, 2014.

[2] H. Hu, F. Hao, X. Guo, F. Dai, Y. Lu, and Y. Ma, "Investigation of methane sorption of overmature Wufeng-Longmaxi shale in the Jiaoshiba area, Eastern Sichuan Basin, China," *Marine and Petroleum Geology*, vol. 91, pp. 251–261, 2018.

[3] H. Hu, T. Zhang, J. D. Wiggins-Camacho, G. S. Ellis, M. D. Lewan, and X. Zhang, "Experimental investigation of changes in methane adsorption of bitumen-free Woodford Shale with thermal maturation induced by hydrous pyrolysis," *Marine and Petroleum Geology*, vol. 59, pp. 114–128, 2015.

[4] L. Ji, T. Zhang, K. L. Milliken, J. Qu, and X. Zhang, "Experimental investigation of main controls to methane adsorption in clay-rich rocks," *Applied Geochemisty*, vol. 27, no. 12, pp. 2533–2545, 2012.

[5] J. Li, S. Zhou, G. Gaus et al., "Characterization of methane adsorption on shale and isolated kerogen from the Sichuan Basin under pressure up to 60 MPa: experimental results and geological implications," *International Journal of Coal Geology*, vol. 189, pp. 83–93, 2018.

[6] H. Tian, T. Li, T. Zhang, and X. Xiao, "Characterization of methane adsorption on overmature Lower Silurian–Upper Ordovician shales in Sichuan Basin, Southwest China: Experimental results and geological implications," *International Journal of Coal Geology*, vol. 156, pp. 36–49, 2016.

[7] T. Zhang, G. S. Ellis, S. C. Ruppel, K. Milliken, and R. Yang, "Effect of organic-matter type and thermal maturity on methane adsorption in shale-gas systems," *Organic Geochemistry*, vol. 47, pp. 120–131, 2012.

[8] T. Zhao, X. Li, Z. Ning, H. Zhao, and M. Li, "Molecular simulation of methane adsorption on type II kerogen with the impact of water content," *Journal of Petroleum Science & Engineering*, vol. 161, pp. 302–310, 2018.

[9] J. Zou, R. Rezaee, Q. Xie, L. You, K. Liu, and A. Saeedi, "Investigation of moisture effect on methane adsorption capacity of shale samples," *Fuel*, vol. 232, pp. 323–332, 2018.

[10] S. Chen, Y. Han, C. Fu, H. Zhang, Y. Zhu, and Z. Zuo, "Micro and nano-size pores of clay minerals in shale reservoirs: implication for the accumulation of shale gas," *Sedimentary Geology*, vol. 342, pp. 180–190, 2016.

[11] D. Cristancho-Albarracin, I. Y. Akkutlu, L. J. Criscenti, and Y. Wang, "Shale gas storage in kerogen nanopores with surface heterogeneities," *Applied Geochemisty*, vol. 84, pp. 1–10, 2017.

[12] Y. Pang, M. Y. Soliman, H. Deng, and X. Xie, "Experimental and analytical investigation of adsorption effects on shale gas transport in organic nanopores," *Fuel*, vol. 199, pp. 272–288, 2017.

[13] Y. Wang, Y. Zhu, S. Liu, and R. Zhang, "Pore characterization and its impact on methane adsorption capacity for organic-rich marine shales," *Fuel*, vol. 181, pp. 227–237, 2016.

[14] D. Z. Ren, L. T. Ma, D. K. Liu, J. Tao, X. Q. Liu, and R. J. Zhang, "Control mechanism and parameter simulation of oil-water properties on spontaneous imbibition efficiency of tight sandstone reservoir," *Frontiers in Physics*, vol. 176, no. 10, article 829763, 2022.

[15] D. Z. Ren, H. P. Zhang, Z. Z. Wang, B. Y. Ge, D. K. Liu, and R. J. Zhang, "Experimental study on microscale simulation of oil accumulation in sandstone reservoir," *Frontiers in Physics*, vol. 176, no. 10, article 841989, 2022.

[16] Z. H. Zhao, K. D. Wu, Y. Fan, J. C. Guo, B. Zeng, and W. H. Yue, "An optimization model for conductivity of hydraulic fracture networks in the Longmaxi shale, Sichuan basin, Southwest China," *Energy Geoscience*, vol. 1, no. 1-2, pp. 47–54, 2020.

[17] J. Li, P. P. Li, S. X. Zhou, Z. X. Sun, B. K. Meng, and Y. Y. Li, "Competitive adsorption of methane and ethane on organic-rich shale at pressure up to 30 MPa: experimental results and geological implications," *Chemical Engineering Journal*, vol. 444, article 136617, 2022.

[18] L. M. Ji, L. Su, Y. D. Wu, and C. He, "Pore evolution in hydrocarbon-generation simulation of organic matter-rich muddy shale," *Petroleum Research*, vol. 2, no. 2, pp. 146–155, 2017.

[19] T. Li, H. Tian, X. Xiao, P. Cheng, Q. Zhou, and Q. Wei, "Geochemical characterization and methane adsorption capacity of overmature organic-rich Lower Cambrian shales in northeast Guizhou region, southwest China," *Marine and Petroleum Geology*, vol. 86, pp. 858–873, 2017.

[20] T. Topór, A. Derkowski, P. Ziemiański, J. Szczurowski, and D. K. McCarty, "The effect of organic matter maturation and porosity evolution on methane storage potential in the Baltic Basin (Poland) shale-gas reservoir," *International Journal of Coal Geology*, vol. 180, pp. 46–56, 2017.

[21] Z. Jiang, L. Zhao, and D. Zhang, "Study of adsorption behavior in shale reservoirs under high pressure," *Journal of Natural Gas Science and Engineering*, vol. 49, pp. 275–285, 2018.

[22] Y. Wang, Y. Zhu, S. Liu, and R. Zhang, "Methane adsorption measurements and modeling for organic-rich marine shale samples," *Fuel*, vol. 172, pp. 301–309, 2016.

[23] R. Yang, S. He, Q. Hu, D. Hu, S. Zhang, and J. Yi, "Pore characterization and methane sorption capacity of over-mature organic-rich Wufeng and Longmaxi shales in the southeast Sichuan Basin, China," *Marine and Petroleum Geology*, vol. 77, pp. 247–261, 2016.

[24] R. M. Bustin and C. R. Clarkson, "Geological controls on coalbed methane reservoir capacity and gas content," *International Journal of Coal Geology*, vol. 38, no. 1-2, pp. 3–26, 1998.

[25] D. Fu, G. Xu, T. Tian, J. Qin, and F. Yang, "Composition of the shales in Niutitang formation at Huijunba syncline and its influence on microscopic pore structure and gas adsorption," *Petrophysics*, vol. 60, pp. 373–383, 2019.

[26] T. Tian, S. Zhou, D. Fu, F. Yang, and J. Li, "Calculation of the original abundance of organic matter at high-over maturity: a case study of the Lower Cambrian Niutitang shale in the Micangshan-Hannan Uplift, SW China," *Journal of Petroleum Science and Engineering*, vol. 179, pp. 645–654, 2019.

[27] J. Yan, T. Zhang, Y. Li, H. Lv, and X. Zhang, "Effect of the organic matter characteristics on methane adsorption in shale," *Journal of the China Coal Society*, vol. 38, pp. 805–811, 2013.